BNL-215891-2020-TECH

NSLSII-ASD-TN-330

Beam-induced Power in HEX Superconducting Wiggler

V. Smaluk

April 2020

Photon Sciences

Brookhaven National Laboratory

U.S. Department of Energy

USDOE Office of Science (SC), Basic Energy Sciences (BES) (SC-22)

DISCLAIMER

NSLS II TECHNICAL NOTE BROOKHAVEN NATIONAL LABORATORY	NUMBER NSLSII-ASD-TN-330
AUTHOR **V. Smaluk, A. Blednykh, C. Hetzel, T. Tanabe**	DATE **04/14/2020**
TITLE **Beam-induced power in HEX superconducting wiggler**	

Abstract

A superconducting wiggler (SCW) is planned to be installed in NSLS-II for HEX beamline. Interaction of the electron beam with the resistive-wall impedance of the low-gap SCW liner and with the geometric impedance of the transition sections results in excitation of electromagnetic fields, dissipation of which heats the vacuum chamber in the cold volume. The beam-induced power caused by the beam-impedance interaction is estimated using analytical formulae and computer simulations for two design options: one from the vendor and one from NSLS-II.

Introduction

The beam-induced heating of the superconducting wigglers and undulators is one of the major design concerns. Detailed experimental and theoretical studies of the beam-induced heat loads in superconducting insertions were carried out at ANKA [1] and Diamond [2] light sources. As it is noticed in [2], the beam heat load predicted considering only resistive wall heating does not fit the experimental data measured in the cold vacuum chamber for diagnostics installed at the Diamond Light Source. The contribution of the geometrical impedance of the thermal transitions is significant.

In this note, we present the heat load assessment for a superconducting wiggler, which will be installed at NSLS-II for the HEX beamline. The heat power resulted from the beam interaction with the geometric and resistive-wall impedance (including normal and anomalous skin effects) is estimated using analytical formulae and numerical simulations.

For all estimations of the beam-induced power, we assume a Gaussian bunch with the shortest possible r.m.s. length of 3 mm (no harmonic cavities, three main RF cavities, high RF voltage). The power is lower for longer bunches.

Coherent energy loss

The power induced by the beam-impedance interaction is calculated by the formula:

$$P = k_{||} \frac{I^2}{N_b f_0}, \tag{1}$$

where I is the average beam current, N_b is the number of bunches in the train, f_0 is the revolution frequency. Here $k_{||}$ is the longitudinal loss factor

$$k_{||} = \frac{1}{\pi}\int_0^{\infty} Z_{||}(\omega)\tilde{\lambda}^2(\omega)d\omega \ , \qquad (2)$$

where $Z_{||}(\omega)$ is the longitudinal impedance and $\tilde{\lambda}(\omega)$ is the bunch spectrum (Fourier transform of the longitudinal bunch profile $\lambda(t)$). For a Gaussian bunch, $\tilde{\lambda}^2(\omega) = e^{-\omega^2\sigma_t^2}$, where $\sigma_t = \frac{\sigma_z}{c}$ and σ_z is the r.m.s. bunch length.

The impedance includes the geometric and resistive-wall components, the first one is obtained by numerical simulations, and the second one is calculated using analytical formulae.

Geometric impedance

The geometric impedance is calculated by Gdfidl code [3] using a simplified model of the SCW vacuum chamber. Two design options were analyzed.

The chamber proposed by NSLS-II Vacuum group includes a 1.65-m long central part with the vertical aperture of 8 mm, two 137-mm long tapered transitions with the vertical aperture changing linearly from $2b = 7$ mm up to $2d = 25$ mm, and two short (12.7 mm) tapered transitions from 7 mm to 8 mm. Fig. 1 shows the model used for the simulation.

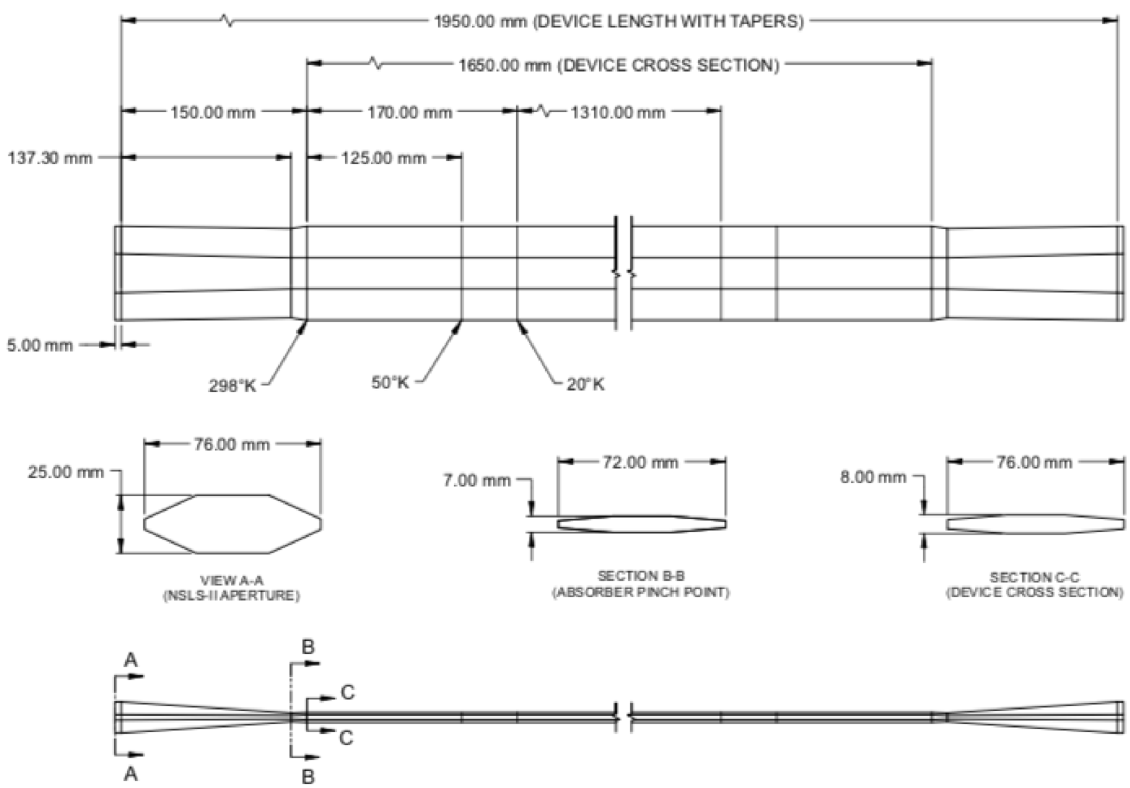

Fig. 1. SCW model used for wakefield simulations (NSLS-II design).

For the chamber proposed by Bilfinger, the central narrow-gap part is 1.556-m long, the tapered transitions are shorter (90 mm), and two bellows with RF shields are included in this design. Fig. 2 shows the model used for the simulation.

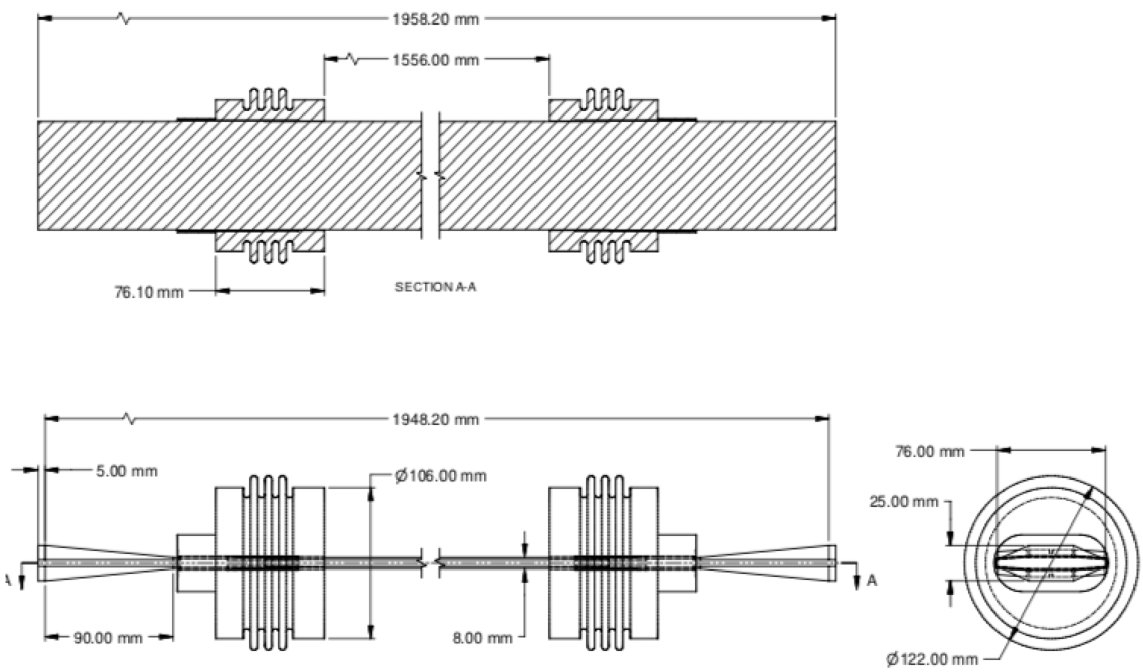

Fig. 2. SCW model used for wakefield simulations (Bilfinger design).

To check the simulation accuracy, the impedance calculated by GdfidL is compared to the analytical formulae. For the tapered transition, the low-frequency normalized longitudinal impedance can be estimated with the formula [4]:

$$\frac{Z}{n} = -i\,\frac{Z_0\omega_0}{4\pi c}\int_{-\infty}^{\infty}(g')^2 F\left(\frac{g}{w}\right)dz\ , \tag{3}$$

where $g' = dg/dz$, $g(z)$ is the taper profile, w is the full width, Z_0 is the free space impedance, $n = \omega/\omega_0$, ω_0 is the cyclic revolution frequency. The function F is defined as

$$F(x) = \sum_{m=0}^{\infty}\frac{1}{2m+1}\operatorname{sech}^2\phi_m\,\tanh\phi_m\ , \qquad \phi_m = (2m+1)\frac{\pi x}{2}\ . \tag{4}$$

The chamber proposed by Bilfinger contains 8 round-ended rectangular slots, the low-frequency normalized impedance of which can be approximately estimated by the formula for a small obstacle [5]

$$\frac{Z}{n} = -i\,\frac{Z_0\omega_0}{96\pi c}\frac{w^4}{b^2 l}\left(\ln\frac{4l}{w} - 1\right)\ , \tag{5}$$

where $l = 20\ mm$ is the slot length, $w = 5\ mm$ is the width, and $b = 4\ mm$ is the vertical half-aperture.

The imaginary part of the simulated geometric impedance of the whole chamber is shown in Fig. 3 together with the inductive impedance calculated using equation (3) for the NSLS-II design (Fig. 3a) and equations (3) and (5) for the Bilfinger design (Fig. 3b). The calculations look consistent, so we can conclude the simulations are accurate enough.

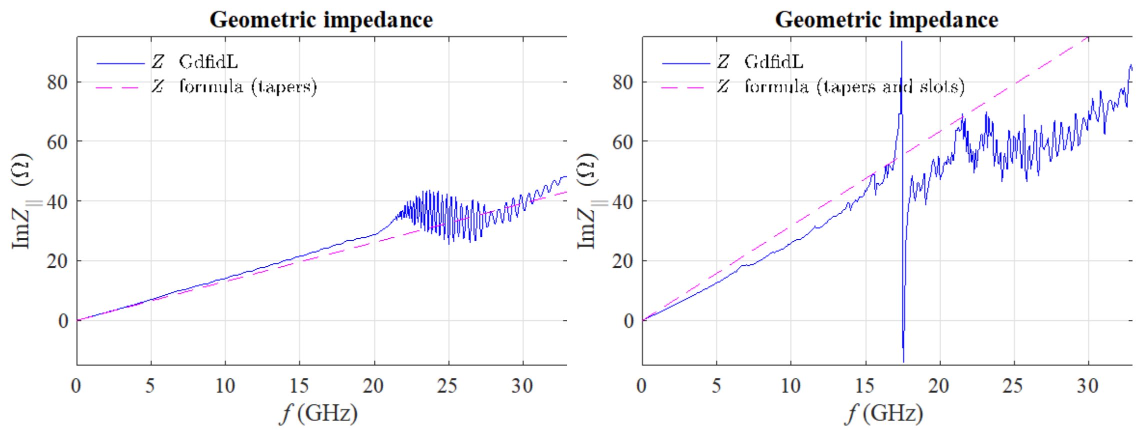

a) NSLS-II b) Bilfinger

Fig. 3. Geometric impedance: simulations vs formula.

The real part of the geometric impedance contributing to the beam power loss is shown in Fig. 4 together with the bunch power spectrum $\tilde{\lambda}^2(\omega)$ calculated for a Gaussian bunch with r.m.s. length $\sigma_z = 3$ mm. Fig. 4a corresponds to the NSLS-II design and Fig. 4b corresponds to the Bilfinger design.

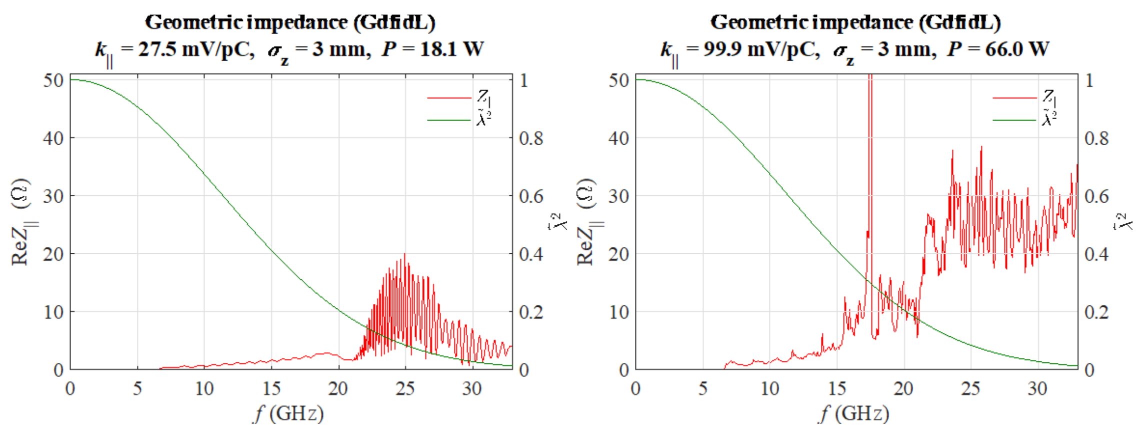

a) NSLS-II b) Bilfinger

Fig. 4. Geometric impedance of SCW model vacuum chamber.

The loss factor calculated using the impedance shown in Fig. 4 and a Gaussian bunch with $\sigma_z = 3$ mm is 27.5 mV/pC for the NSLS-II design and 100 mV/pC for the Bilfinger design. For the total beam current of $I = 500$ mA in $N_b = 1000$ bunches, the beam-induced power is 18 W and 66 W, respectively.

The presence of HOMs in the Bilfinger structure is due to the flange joints, those are not RF shielded, the strongest resonance peak is at the frequency of 17 GHz, other resonance modes are caused by the bellows geometry and the tapered transitions.

Resistive-wall impedance of the tapered transitions (normal skin effect)

To estimate the contribution of the tapered transitions, we assume they are normal-conducting copper plates. If the transition is modeled by two infinite plates, the longitudinal resistive-wall impedance per unit length $Z_{||}/L$ is:

$$Z_{||}/L = \frac{1-i}{2\pi b}\sqrt{\frac{Z_0\mu_r\omega}{2c\sigma_c}}\,, \tag{6}$$

here b is the vertical half-aperture. Following the impedance, the beam-induced power per unit length $P_{||}/L$ is inversely proportional to the aperture, as shown in Fig. 5.

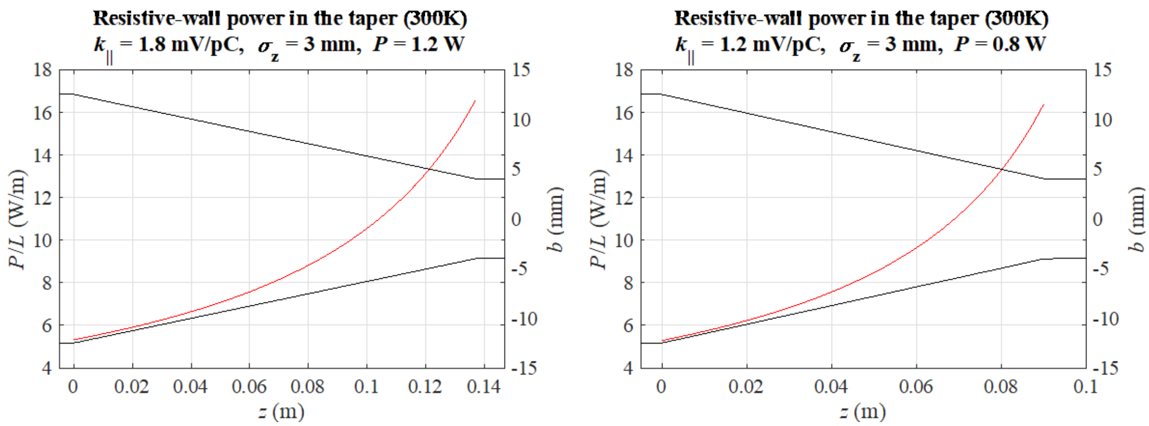

a) NSLS-II b) Bilfinger

Fig. 5. Beam-induced power: resistive-wall impedance of one tapered transition.

Assuming a Gaussian bunch with $\sigma_z = 3$ mm the loss factor is 1.8 mV/pC (NSLS-II) and 1.2 mV/pC (Bilfinger). For one transition, the integrated power is 1.2 W (NSLS-II) and 0.8 W (Bilfinger); $I = 500$ mA and $N_b = 1000$.

Resistive-wall impedance of the liner (anomalous skin effect)

To calculate the resistive-wall impedance of the superconducting copper liner (anomalous skin effect), a set of formulae published in [6] is used. For a round vacuum chamber, the longitudinal coupling impedance per unit length $Z_{||}/L$ is proportional to the surface impedance Z_s:

$$Z_{||}/L = \frac{Z_s}{2\pi b}\,, \tag{7}$$

where b is the chamber radius. The real part of the surface impedance Z_s is the surface resistance

$$R_s = \sqrt[3]{\frac{\sqrt{3}Z_0^2\omega^2}{16\pi c^2}\, l/\sigma_c}\,\left(1 + 1.157\varsigma^{-0.2757}\right)\,, \tag{8}$$

where $\varsigma = \frac{3}{2}\left(\frac{l}{\delta_s}\right)^2$, l is the electron mean free path, $\delta_s = \sqrt{\frac{2c}{Z_0\mu_r\sigma_c\omega}}$ is the skin depth, $Z_0 = 377\Omega$ is the free-space impedance, μ_r is the relative permeability, σ_c is the conductivity. The ratio l/σ_c is independent of temperature, $l/\sigma_c = 6.6\cdot 10^{-16}\Omega\mathrm{m}^2$ for copper. Formula (8) is valid for $\varsigma \geq 3$. If $l \gg \delta_s$ (extreme anomalous skin effect), the second term in the brackets becomes negligible and the surface resistance is

$$R_{s\infty} = \sqrt[3]{\frac{\sqrt{3}Z_0^2\omega^2}{16\pi c^2}\, l/\sigma_c}\,. \tag{9}$$

At cryogenic temperatures, the conductivity is proportional to the residual resistivity ratio defined as $RRR = \frac{\rho(273\text{ K})}{\rho(4.2\text{ K})}$. Commercially pure copper has the residual resistivity ratio of 50 to 500, whereas very high-purity copper, well-annealed, could have an RRR of around 2000 [7]. Electrical resistivity of annealed oxygen-free copper is shown in Fig. 6 as a function of temperature. Several curves corresponding to RRR from 30 to 3000 are presented.

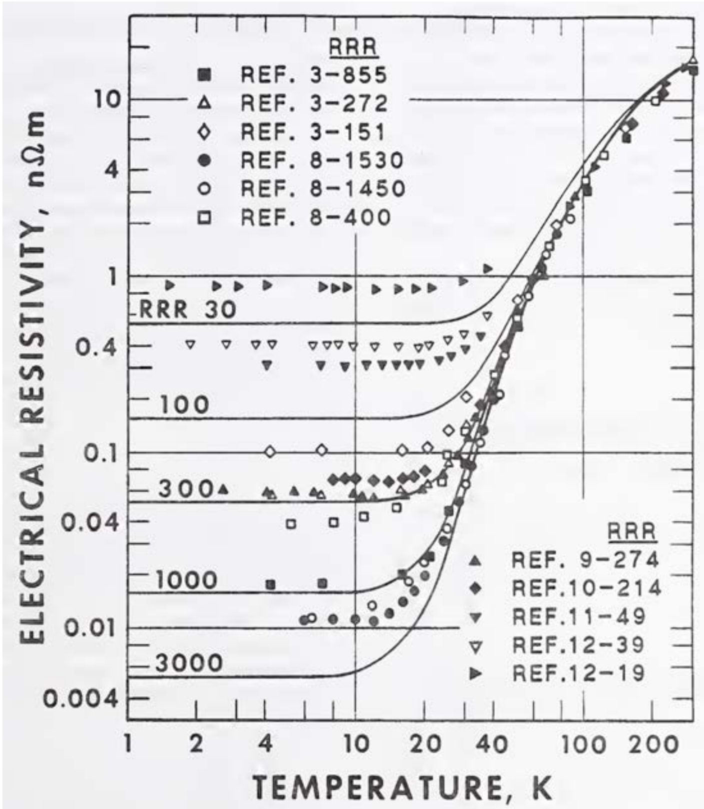

Fig. 6. Resistivity of annealed oxygen-free copper as a function of temperature.

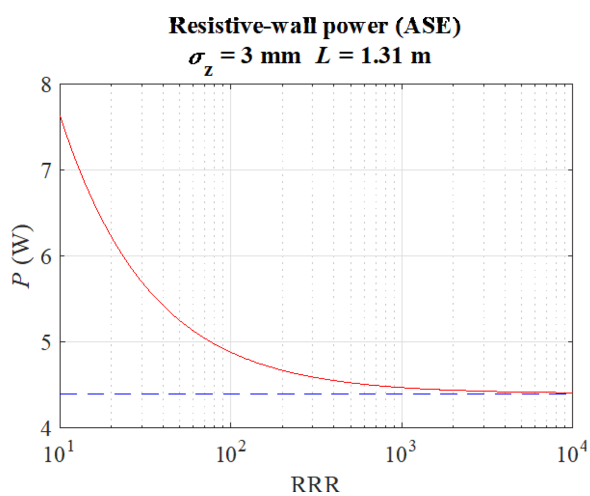

Fig. 7. Beam-induced power: resistive-wall impedance of the cold liner.

Fig. 7 shows the beam-induced power (1) as a function of the residual resistivity ratio. The calculations are done for the cold chamber with the length of 1.3 m and the full gap of

8 mm using NSLS-II machine and beam parameters: $I = 500$ mA, $N_b = 1000$, $f_0 = 378.6$ kHz, $\sigma_z = 3$ mm. The dashed line represents the power calculated in the limit of extreme anomalous skin effect.

Transitions between the warm and cold parts

The constant-aperture transition from the warm part (300 K) to the cold (20 K) part of the chamber is 170-mm long (see Fig. 1). The simulated temperature distribution along the transition is shown in Fig. 8.

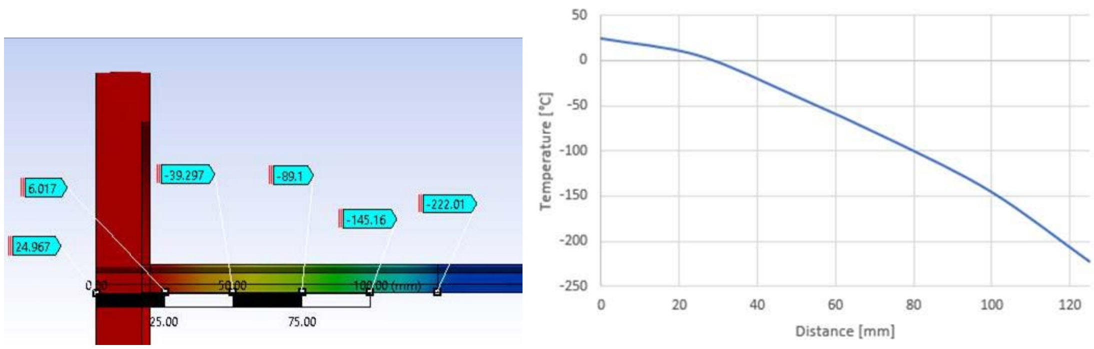

Fig. 8. Temperature distribution along the transition.

Assuming the same warm-to-cold transitions for both NSLS-II and Bilfinger chambers, the power per unit length along the transition is calculated using formulae (1-3) assuming the conductivity σ_c dependent of the longitudinal coordinate according to the curves shown in Fig. 6 and Fig. 8. The power per unit length is shown in Fig. 9 together with the temperature-dependent resistivity.

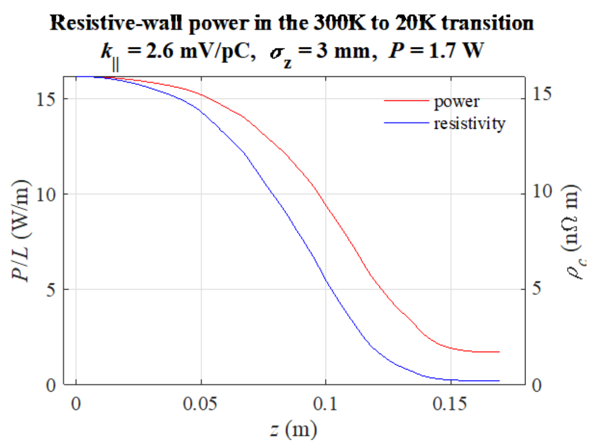

Fig. 9. Power per unit length and resistivity along the warm-to-cold transition.

For the same beam parameters ($\sigma_z = 3$ mm, $I = 500$ mA, $N_b = 1000$), the integrated power is about 1.7 W for one transition.

Total beam-induced power

Combining the contributions from both geometric and resistive-wall impedance including the cold liner, two warm tapered transitions, and two transitions from 300 K to 20 K, we estimate the total beam-induced power in the HEX SCW. Fig. 10 shows the power as a function of the r.m.s. bunch length for the NSLS-II design (blue line) and for the Bilfinger design (red line). For the cold liner, the resistive-wall impedance is calculated assuming RRR=100. The total beam current is 500 mA, the number of bunches is 1000.

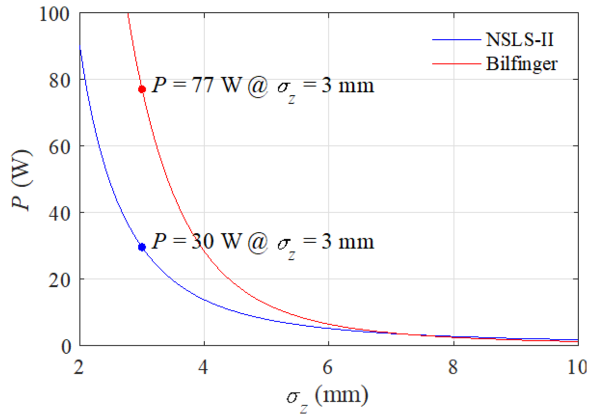

Fig. 10. Total beam-induced power.

For the r.m.s. bunch length of 3 mm, the total power is estimated as 30 W (NSLS-II design) and 77 W (Bilfinger design).

The power induced by the beam interaction with geometric impedance is not necessarily to dissipate where the wakefields are generated, a part of it can propagate in the vacuum chamber and dissipate in other locations.

Note that having such a risky element as bellows in the cold volume can be dangerous. The impedance is calculated assuming perfect contact of the RF fingers. In a possible case of poor contact, a contact arc can occur, or the beam will interact with the "unshielded" bellows having much higher impedance than the RF-shielded one. Any of these effects can suddenly increase the heat load resulting in quenches.

References

1. S. Casalbuoni, A. Grau, M. Hagelstein, et al, "Beam heat load and pressure rise in a cold vacuum chamber", Phys. Rev. ST Accel. Beams 10, 093202 (2007).

2. R. Voutta, S. Gerstl, S. Casalbuoni, et al, "Cold vacuum chamber for diagnostics: Analysis of the measurements at the Diamond Light Source and impedance bench measurements", Phys. Rev. ST Accel. Beams 19, 053201 (2016).

3. The GdfidL Electromagnetic Field simulator, http://www.gdfidl.de/

4. G. Stupakov, "Low frequency impedance of tapered transitions with arbitrary cross sections", Phys. Rev. ST Accel. Beams 10, 094401 (2007).

5. S. Kurennoy, "Beam-Chamber Interaction in Accelerators. Methods for Calculating Coupling Impedances", Phys. Elem. Part. At. Nucl. 24 (3), 878 (1993).

6. G. E. H. Reuter and E. H. Sondheimer, "The theory of the anomalous skin effect in metals", Proc. R. Soc. A 195, 336 (1948).

7. N. J. Simon, E. S. Drexler, and R. P. Reed, "Properties of Copper and Copper Alloys at Cryogenic Temperatures", NIST Monograph 177 (1992) p. 301